

A UK local seismic magnitude scale, ML^P , using P -wave amplitudes

David N. Green¹,^{ORCID} Richard Lockett,² Brian Baptie² and David Bowers¹

¹*AWE Blacknest, Brimpton, Reading, RG7 4RS, UK. E-mail: dgreen@blacknest.gov.uk*

²*British Geological Survey, Earthquake Seismology, The Lyell Centre, Edinburgh, EH14 4AP, UK*

Accepted 2020 September 15. Received 2020 September 10; in original form 2020 February 7

SUMMARY

A local seismic magnitude scale, ML^P , has been developed for the United Kingdom (UK) using automated measurements of 8902 half peak-to-peak vertical component seismic P -wave displacement amplitudes from 630 earthquakes. The measurement time window increases with source-to-receiver range such that ML^P is sensitive to the dominant phase within the P -wavetrain at a given distance. To avoid contamination due to low-frequency noise, the P -wave amplitude measurements are made in the 1.5–30 Hz passband. A least-squares inversion was undertaken to estimate source size, distance and station effects. The distance effect values suggest that P -wave amplitude attenuation across the UK is low when compared to other tectonically stable regions. The station effects are broadly consistent with UK geology, with signal amplification observed within the sediments towards the south-east of the country. ML^P has been tied to the UK local magnitude scale routinely estimated by the British Geological Survey (BGS, determined using S waves, and here denoted ML^{BGS}). For earthquakes with $ML^{BGS} > 3$, ML^P exhibits a closer correspondence to the moment magnitude than ML^{BGS} (i.e. $ML^P \approx M_w$). It is tentatively suggested that this reduction in bias is caused by the P -wave scale being less affected by along-path attenuation. The difference with respect to physical source scaling helps explain the divergence of the ML^{BGS} and ML^P scales at $ML > 3$. ML^P allows a robust estimate of event size to be made for small events which predominantly generate P waves, for example, near-surface explosions. ML^P values have been calculated for 239 explosive events, mostly mining blasts and munitions disposal. Although there is significant scatter, explosive events exhibit elevated ML^P values compared to ML^{BGS} , consistent with explosions generating proportionally more compressional wave energy than earthquakes. For example, 33 explosions at sea exhibit a median $ML^P - ML^{BGS}$ value of 0.50 mag units. Despite its sensitivity to P -wave amplitude, ML^P is not a more consistent estimator of explosive source size than ML^{BGS} ; the magnitude residuals (station estimate – event estimate) are slightly less for ML^{BGS} compared to ML^P . This is primarily due to variability of the P -wave amplitudes that cannot be explained by a 1-D distance correction. ML^P should be considered as an additional tool for characterizing small seismic events within the UK.

Key words: Body waves; Earthquake source observations; Site effects.

1 INTRODUCTION

Seismic magnitude scales, based on measurements of signal amplitudes, provide an easy-to-calculate measure of relative seismic event size. Despite the difficulties in relating local seismic magnitude scales to physical measures of source size (e.g. Deichmann 2006, 2017; Dost *et al.* 2018), magnitudes remain relevant as they provide continuity with past measurements.

Local magnitude procedures most often utilize measurements of the maximum amplitude signal arrival in a given passband (e.g. Richter 1935). For earthquakes this is usually, depending on propagation distance, the S or L_g arrival. However, for explosive sources

the P wave often contains the highest amplitude arrival at local distances. For example, P -wave arrivals exhibited the largest amplitudes within the seismic wavetrain out to distances of at least 240 km from a UK oil depot explosion (Ottemöller and Evers 2008). Local magnitude calculation procedures which rely on maximum amplitude measures across a seismometer network may therefore utilize a mixture of phases, especially for explosive events.

Given that local magnitude procedures are likely to have been constructed using S - and L_g -wave amplitudes from earthquakes, these magnitude scales have amplitude decay terms that reflect S -wave attenuation and station-specific terms that reflect near receiver S -wave responses. In this paper seismic data collected by the

British Geological Survey (BGS) is used to construct a magnitude scale, ML^P , that incorporates only P -wave amplitude measurements. The results are compared to the local magnitude scale, here denoted ML^{BGS} , routinely used by the BGS when describing seismic event sizes in the United Kingdom (UK, Ottemöller & Sargeant 2013). The aims of constructing the ML^P scale are twofold: (1) to test the hypothesis that measuring P -wave amplitudes will produce a reliable measure of source size, and (2) to construct a scale that will be applicable for the analysis of small near-surface explosions for which P -wave arrivals dominate recordings across a local (or near-regional) network.

2 DATA SET

Earthquake recordings held in the BGS seismic waveform database, spanning the time period 1990–2015 inclusive, were used to develop the ML^P magnitude scale. Only earthquake signals were used in the inversion for the ML^P scale parameters, and the results of the inversion were subsequently tested using a small set of explosively generated signals to determine whether ML^P exhibits any power to discriminate between different source types. These two data sets are described below.

Signals used within the ML^P inversion were generated by earthquakes that predominantly occurred within the mid-crust, with the distribution of depths having a median value of 7.7 km (and 5th/95th percentile depths of 1.5 and 22 km, respectively). The observations were made across regional stations that the BGS utilize in their monitoring operations. These stations include the BGS network (both short-period and broad band), UKNET sites run by AWE Blacknest (e.g. Douglas 2001), and selected stations in Ireland (see Fig. 1). Not all stations were operational across the entire 1990–2015 time period, nor were all events recorded at all operational stations.

Only (presumed) earthquakes with $ML^{BGS} > 2.0$ were used in the construction of ML^P , as small earthquakes are often observed at few stations with waveforms exhibiting poor signal-to-noise ratios. Further quality control steps were undertaken to reduce the effect of single amplitude measurements on poorly constrained parameters: (1) stations which observed less than three measurements across the data set were discarded, (2) events which had less than three arrivals across the network were removed and (3) analysis was restricted to signals with source-to-receiver path lengths less than 990 km. This process resulted in a data set that contained 8902 observations from 630 events across 181 stations (for the 1.5–30 Hz frequency band studied in this paper, see Section 3.1). No known explosions or quarry blasts were included in this data set.

To study the effect of source characteristics, ML^{BGS} and ML^P magnitudes were also calculated for a BGS data set of explosively generated signal waveforms. Due to the small number and size of explosive events that are seismically recorded across the UK, events with $ML^{BGS} \geq 0.6$ from the period 1989–2014 were investigated. This allowed a data set of 239 events to be constructed containing four classes of explosions (Table 1). Quarry blasts within the data set were split into two groups to highlight events occurring at Glensanda Quarry, Scotland (56.588°N, 5.564°W), for which explosive charge weights are reported by Booth (2009). A consequence of having to use such small events ($ML^{BGS} \geq 0.6$), is that the robustness of any magnitude estimate needs to be considered during interpretation. P -wave amplitude estimates could not be made for events that occurred earlier than 1989; waveforms were not available.

3 METHODOLOGY

3.1 Automatic P -wave amplitude picks

To generate a UK ML^P magnitude scale an algorithm was developed to automatically measure vertical component P -wave half peak-to-peak displacement amplitudes. All input data traces were transformed to displacement through deconvolution of the instrument response. A variety of frequency passbands were tested during an initial analysis, as it may have been advantageous to use passbands utilized by other magnitude scales for comparative purposes. However, amplitudes measured for smaller events ($ML^{BGS} < 3$) were contaminated by low-frequency noise (i.e. < 1 Hz). Therefore, all analysis in this paper is conducted in a passband of 1.5–30 Hz.

The measurement algorithm identifies half peak-to-peak displacement amplitudes within a pre-defined window around an analyst P -wave pick. To identify the most suitable window, a number of possible choices (test windows) were tested on a subset of 29 events from the data set. These test windows included: constant duration windows, windows whose duration depended upon source-to-receiver distance and windows that were time-localized in an attempt to capture either P_g or P_n energy depending on distance from the source. For each test window, P waves were automatically measured on the vertical component seismograms using the following steps (see Fig. 2):

- (i) The absolute maximum displacement amplitude (A_1) in the window was identified.
- (ii) A truncated window was isolated between the time of A_1 up to the time at which zero displacement is crossed for the second time.
- (iii) The largest amplitude, A_{after} , with the opposite sign to the absolute maximum was found in this truncated window.
- (iv) Steps 2 and 3 were repeated within a truncated window for times before the absolute amplitude maximum, providing an amplitude value A_{before} .
- (v) The largest of the two amplitudes, A_{after} and A_{before} , was taken as the second extreme value, A_2 .
- (vi) The half peak-to-peak amplitude was calculated as $(|A_1| + |A_2|)/2$.

The window used to measure amplitudes for the ML^P calculations was chosen to be the test window which resulted in the smallest variance for the amplitude residual population, where the residual was defined as $|\text{measured} - \text{predicted amplitude}|$. The amplitude predictions were made using a seismic amplitude model for which the parameters were estimated via a least-squares inversion constrained by the measured amplitudes. The seismic amplitude model has the form (e.g. Carpenter *et al.* 1967; Booth 2007),

$$\log_{10} A = b + s + r, \quad (1)$$

where A is the seismic amplitude, b is a source size effect, s is a station effect and r is a distance effect. The chosen window starts 0.2 s prior to the analyst pick and has a duration in seconds equal to 0.09 multiplied by the source-to-receiver range in kilometres. The chosen window exhibited summed squared residuals (χ^2) between the observed and predicted amplitudes which were at least 35 per cent smaller than those calculated for the other test windows.

The combination of the P -wave analyst pick and choice of window are approximately equivalent to a constant group velocity window for the epicentral distance ranges in which either P_g or P_n is expected to be the first arrival. If the P -wave pick is equivalent to a group velocity of 6.0 km s⁻¹ (appropriate for UK P_g arrivals, e.g. Bamford *et al.* 1978), the end of the window will occur at a time

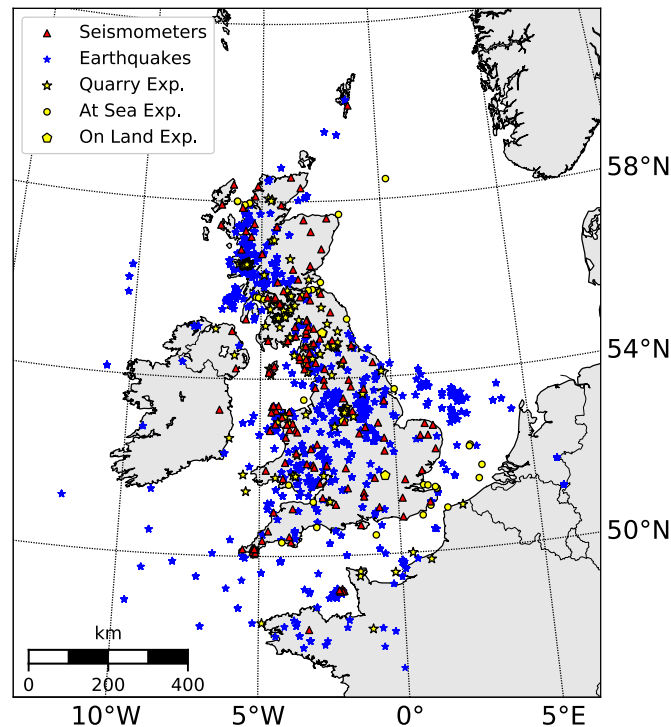


Figure 1. The earthquakes (blue stars), explosions (yellow symbols) and stations (red triangles) used within this study. Note that not all stations were operational across the entire 1990–2015 time period considered, nor were all events recorded at all operational stations.

Table 1. The explosion database.

Class	Number of events	ML ^{BGS} range
Quarry Blasts (non Glensanda quarry)	190	[0.9,2.7]
Glensanda quarry blasts	13	[1.5,1.7]
At sea	33	[1.0,3.4]
On land (non-quarry)	3	[0.6,2.3]

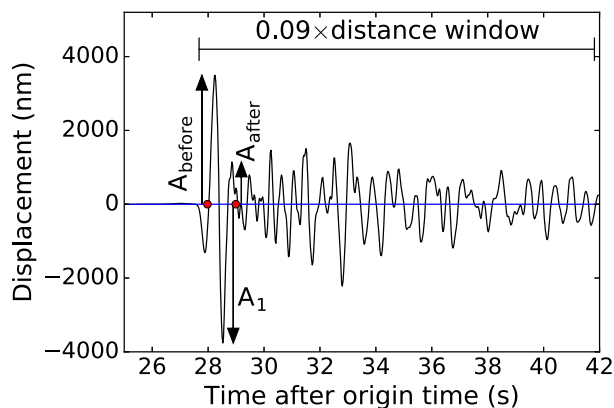


Figure 2. A cartoon illustrating the automatic amplitude measurement technique, using data from the ML^{BGS} 4.3 2007-Apr-28 Folkestone Earthquake, recorded at station WOL at a distance of 157 km. The maximum absolute amplitude (A_1) is found in the signal window, and then a truncated window either side of this pick is constructed (denoted by region between the two red dots) in order to identify the larger of the two amplitudes, A_{before} and A_{after} .

equivalent to a group velocity of 3.9 km s^{-1} (faster than anticipated S_g arrivals). Likewise, if the P -wave pick is equivalent to a group velocity of 8.0 km s^{-1} (appropriate for UK P_n arrivals) the end time

of the window is equivalent to a group velocity of 4.7 km s^{-1} (faster than anticipated S_n).

It is noted that such a choice of window makes little sense at very short epicentral ranges; the window length tends to zero as the epicentral range decreases to zero. However, by an epicentral range of 10 km the window length is 0.9 s, allowing a robust amplitude measure to be made. Less than 0.5 per cent of observations in this study have epicentral ranges less than 10 km. In addition, at such short epicentral distances magnitude estimates are further complicated by complex propagation effects (e.g. Butcher *et al.* 2017; Luckett *et al.* 2019) and should be interpreted with caution.

The consequence of using the chosen window is that the ML^P magnitude scale is based upon a mixture of P_g and P_n arrival amplitudes. At the shorter source-to-receiver ranges ($\leq 400 \text{ km}$) that will dominate the ML^P estimates the scale will be predominantly based upon measurements of the P_g phase amplitudes, rather than the P_n measurements that are more commonly used to calculate m_b (P_n) magnitudes (e.g. Vergino & Mensing 1990). However, we note that there is precedent for using P_g ; Nuttli (1980) used P_g phases successfully in a study of earthquake magnitudes in Iran.

The automatically measured P -wave amplitudes compared favourably to analyst made measurements in the 1.5–30 Hz pass-band, where distortion due to high amplitude microseismic noise is minimized.

3.2 Magnitude scale estimation

A model for seismic amplitudes of the form in eq. (1) is assumed. No correction is made to the amplitudes for the dominant period of measurement; the scatter in magnitude calculations for other *P*-wave-based regional magnitude scales was reduced by using amplitude rather than the ratio of amplitude and period (e.g. Denny *et al.* 1987).

Given a series of events that generate signals across a sensor network, the resulting amplitude measurements ($a_{ijk} = \log_{10} A_{ijk}$) can be described by the series of equations,

$$a_{ijk} = b_i + s_j + r_k + c + \epsilon_{ijk}, \quad (2)$$

where the subscripts refer to the i^{th} source, the j^{th} station and the k^{th} distance bin, respectively. The distance effect, r , is assumed to be constant over short distance intervals, such that each measurement can be assigned to a particular distance bin (30 km wide bins are used in this analysis). Because the equations of condition for this problem are linearly dependent, a constraint must be added in order to make the problem tractable; here, the average effects are forced to equal zero, that is,

$$\sum_i b_i = \sum_j s_j = \sum_k r_k = 0, \quad (3)$$

requiring that the constant c is added to eq. (2). In addition, an error term, ϵ_{ijk} , is included to reflect the fact that the measurements of amplitude will include some error and the model may not capture all the physical effects.

In order to estimate the parameters b_i , s_j , r_k and c , eq. (2) is solved using least-squares methods (see e.g. Douglas 2013, chapter 2). In the case presented here, with n amplitude observations and p unknowns, the equations of condition can be described by,

$$\mathbf{X}\beta + \epsilon = y, \quad (4)$$

where y is a $n \times 1$ observations vector, \mathbf{X} is an $n \times p$ coefficient matrix and β is a $p \times 1$ vector of unknowns. The p normal equations can then be written as,

$$\mathbf{X}^T \mathbf{X} \hat{\beta} = \mathbf{X}^T y, \quad (5)$$

where T indicates the matrix transpose, and $\hat{}$ indicates an estimate. Note that the constraints (eq. 3) are added via the method of Lagrangian multipliers (see appendix B of Douglas 2013). The solution of eq. (5) can be written as,

$$\hat{\beta} = \mathbf{G}^{-1} \mathbf{X}^T y, \quad (6)$$

where \mathbf{G}^{-1} is the inverse of $\mathbf{X}^T \mathbf{X}$.

To calculate the confidence limits for the parameter estimates we follow the procedure summarized of Douglas (2013, p. 60). The variance of the error in the observations, σ^2 , is not known *a priori* and is therefore estimated from the residuals between predictions and observations,

$$\hat{\sigma}^2 = (y - \mathbf{X}\hat{\beta})^T (y - \mathbf{X}\hat{\beta}) / (n - p). \quad (7)$$

As $\hat{\sigma}^2$ is only an estimate of σ^2 it will be in error. Therefore, the 95 per cent confidence limits on $\hat{\beta}$ are calculated as $\pm t_{95, n-p} \hat{\sigma} \sqrt{s_{jj}}$, where $t_{95, n-p}$ is Student's t at the 95 per cent probability level for $n - p$ degrees of freedom, and s_{jj} is the j^{th} diagonal element of \mathbf{G}^{-1} .

Finally, we wish to compute a seismic magnitude value given our estimates of the source size, distance and station effects. The local magnitude scale, ML (Richter 1935), can be described as,

$$\text{ML} = \log_{10} A - \log_{10} A_0, \quad (8)$$

where $-\log_{10} A_0$ is a correction for the effect of distance, often termed $B(\Delta)$. Following the notation of Booth (2007) we add a station term, S , to allow for possible local station effects, such that

$$\text{ML} = \log_{10} A + B(\Delta) + S. \quad (9)$$

Re-arranging gives,

$$\log_{10} A = \text{ML} - B(\Delta) - S, \quad (10)$$

which shows that $\log_{10} A$ can be expressed as a sum of effects of source size (ML), distance ($B(\Delta)$) and recording site (S), as was assumed for the seismic amplitude model in eq. (2).

For the distance correction we add a constant term, D , such that the magnitudes, ML, calculated using the revised decay curve agree on average with magnitudes computed on another specified magnitude scale, such that,

$$B(\Delta) = -r_k + D. \quad (11)$$

The station correction, S , equals $-s_j$, such that eq. (9) can be reformulated as,

$$\text{ML} = \log_{10} A - r_k + D - s_j. \quad (12)$$

Using eq. (2) this can be simplified to,

$$\text{ML} = b_i + c + D. \quad (13)$$

Here, the value of D is chosen to ensure that ML computed using P , that is, ML^P , is on average the same as that calculated by the ML^{BGS} scale, derived from measurements of maximum horizontal component phase amplitudes (that are predominantly associated with L_g phases, Ottemöller & Sargeant 2013). Therefore, equating the mean magnitude values across both scales leads to,

$$\frac{1}{N} \sum_{i=1}^N \text{ML}_i^{\text{BGS}} = \frac{1}{N} \sum_{i=1}^N \text{ML}_i^P, \quad (14)$$

$$= \frac{1}{N} \sum_{i=1}^N (b_i + c + D), \quad (15)$$

$$= \left(\frac{1}{N} \sum_{i=1}^N b_i \right) + c + D, \quad (16)$$

such that by simple re-arrangement D can be calculated using (1) the estimates of source size from the *P*-wave measurements, b_i , (2) the constant c added to make the problem tractable and (3) the ML^{BGS} magnitude estimates.

4 RESULTS

Using *P*-wave amplitudes measured from the BGS earthquake database (Section 2), the source size, distance and station effects for a *P*-wave amplitude model (eq. 2) were estimated via least-squares inversion (eq. 6). These effects were subsequently converted into corrections for a *P*-wave magnitude scale, ML^P (eq. 9).

4.1 Source size, distance and station effects

Summaries of the three effects, and their variations, are shown in Fig. 3. Variations in source size effects estimated from *P*-wave amplitudes are, as expected, related to variations in ML^{BGS} (Fig. 3b), that is, larger earthquakes produce higher amplitude *P* and L_g phases.

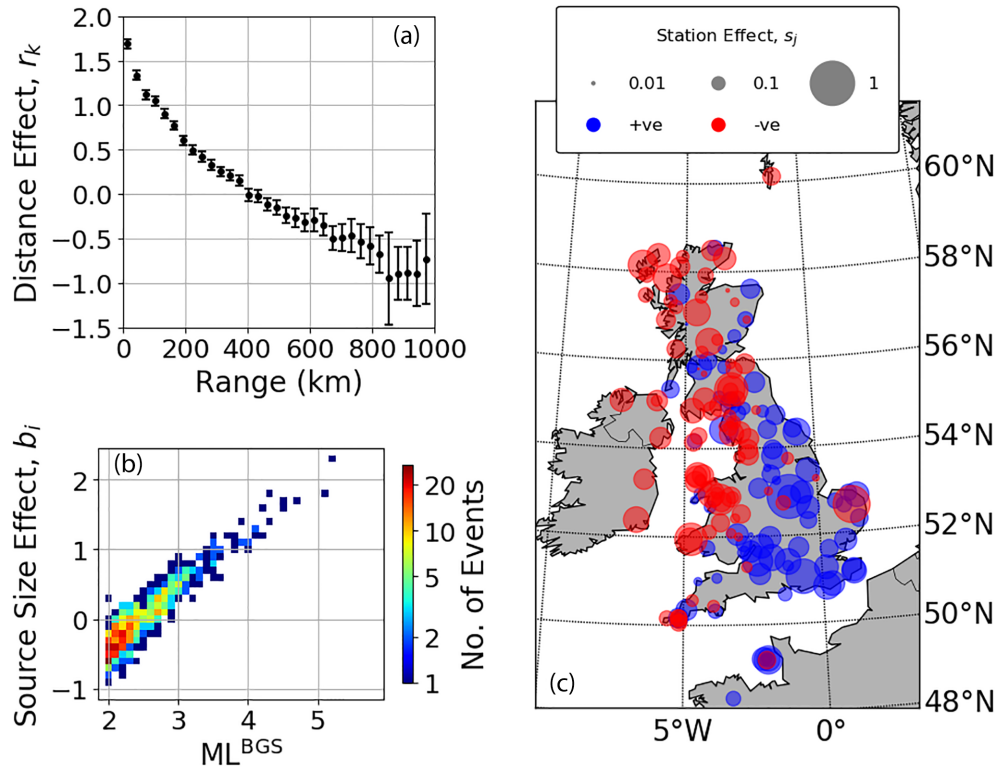


Figure 3. The separated magnitude effects: (a) distance effects showing reduction with source-to-receiver range (error bars represent the 95 per cent confidence limits), (b) source size effects showing increase with seismic event size (as measured by ML^{BGS}) and (c) the geographical variation of station effects.

Geometric spreading and inelastic attenuation of P -wave phases result in a decreasing distance effect, r_k , with increasing source-to-receiver range (Fig. 3a). This translates into a distance correction, $B(\Delta)$, that increases with range (Table 2 and Fig. 4). Note that to ensure that ML^P and ML^{BGS} results are, on average, consistent, $B(\Delta) = -r_k + 1.92$; that is, $D = 1.92$ in eq. (11).

Many previous authors have assumed functional forms for the amplitude decay with distance that can be related to simple models of geometric spreading and attenuation (e.g. Bakun & Joyner 1984). Indeed, the ML^{BGS} scale (Ottmöller & Sargeant 2013) assumes a signal amplitude decrease with distance from the epicentre of the form $A = e^{-\gamma R/R^n}$, where R is the epicentral distance (in km), n is a geometrical spreading coefficient and γ is related to the anelastic attenuation coefficient, Q , by $\gamma = \pi f/Qv$. f and v are wave frequency and velocity, respectively. Such an assumption leads to a distance correction of the form $n \log_{10} R + KR$ where $K = \gamma/\ln 10$. Fitting such a function to our $B(\Delta)$ estimates for ranges between 30 and 750 km results in the relationship (Fig. 4),

$$B(\Delta) = 0.86 \log_{10} R + 0.0014R - 0.95, \quad (17)$$

such that at these ranges ML^P can be approximated as

$$ML^P = \log_{10} A + 0.86 \log_{10} R + 0.0014R - 0.95 + S. \quad (18)$$

The minimum range of 30 km is a conservative choice, reflecting the fact that the $B(\Delta)$ value for the 0–30 km range bin contains very short epicentral distances for which local magnitude estimates have been shown to become less reliable (e.g. Butcher *et al.* 2017; Luckett *et al.* 2019). Indeed, station magnitude residuals, defined as single station magnitude – averaged event magnitude, increase

at epicentral distances of < 10 km with the standard deviation of ML^P magnitude residuals at this range (0.41 m.u.) being approximately 45 per cent larger than standard deviations calculated for 10 km wide bins at epicentral distances of between 10 and 100 km (~ 0.28 m.u.). It is noted for completeness that this short epicentral distance increase in magnitude residual for ML^P is significantly less than that for ML^{BGS} , for which the magnitude residual standard deviation is 0.91 m.u. for epicentral distances < 10 km compared to ~ 0.27 m.u. for 10 km wide bins between 10 and 100 km.

Other authors have fit functions of the form $a \log_{10} R + b$ to restricted distance ranges where a logarithmic relationship between epicentral distance and amplitude decay holds (e.g. Nuttli 1980; Assumpção 1983). For comparison, fitting such a function to our $B(\Delta)$ estimates for epicentral distances, R , between 100 and 750 km allows ML^P to be approximated at these distances as,

$$ML^P = \log_{10} A + 1.84 \log_{10} R - 2.91 + S. \quad (19)$$

The station effects (Fig. 3c) exhibit values distributed around zero with a standard deviation of 0.21 m.u. (Fig. 5b), comparable in amplitude to the error terms, ϵ_{ijk} (standard deviation of 0.25 m.u., Fig. 5a). Nevertheless, the station effects display a clear geographical variation: positive station effects, indicating higher than average P -wave amplitudes, are located predominantly to the south-east of the UK, while negative station effects, indicating lower than average P -wave amplitudes are located predominantly to the north-west of the UK (Fig. 3c). Although the number of observations per station ranges between 3 and 267, the geographical pattern is observed to be robust even at stations with few observations. Furthermore,

Table 2. Distance corrections, $B(\Delta)$, used in the formulation of ML^P (eq. 9) and the associated 95 per cent confidence intervals.

Distance (km)	$B(\Delta)$ (m.u.)	95 per cent C.I. (m.u.)	Distance (km)	$B(\Delta)$ (m.u.)	95 per cent C.I. (m.u.)
0–30	0.23	0.18,0.29	510–540	2.16	2.07,2.24
30–60	0.59	0.54,0.64	540–570	2.18	2.08,2.29
60–90	0.80	0.75,0.86	570–600	2.24	2.14,2.33
90–120	0.87	0.82,0.92	600–630	2.21	2.08,2.34
120–150	1.02	0.97,1.07	630–660	2.27	2.14,2.39
150–180	1.15	1.10,1.20	660–690	2.42	2.28,2.55
180–210	1.31	1.26,1.36	690–720	2.41	2.26,2.56
210–240	1.42	1.37,1.48	720–750	2.38	2.19,2.57
240–270	1.50	1.44,1.55	750–780	2.45	2.25,2.65
270–300	1.59	1.53,1.65	780–810	2.51	2.30,2.72
300–330	1.67	1.61,1.73	810–840	2.59	2.38,2.81
330–360	1.71	1.65,1.77	840–870	2.87	2.36,3.38
360–390	1.77	1.71,1.83	870–900	2.81	2.51,3.11
390–420	1.93	1.87,2.00	900–930	2.81	2.51,3.10
420–450	1.94	1.87,2.02	930–960	2.81	2.45,3.18
450–480	2.03	1.96,2.11	960–990	2.65	2.15,3.16
480–510	2.07	1.99,2.15			

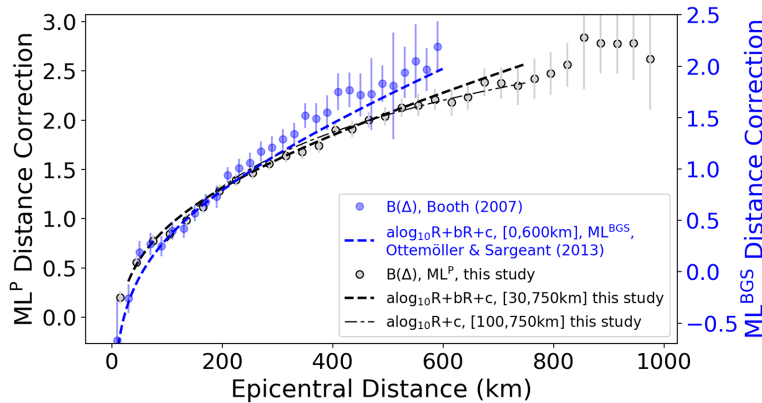


Figure 4. The distance corrections, $B(\Delta)$, as a function of distance, R , for both ML^P and ML^{BGS} relationships. In addition, the distance correction function $0.95\log_{10}R+0.000183R-1.76$ of Ottemöller & Sargeant (2013) is shown. Similar functional relationships have been fit to the ML^P $B(\Delta)$ coefficients, and are described in the text.

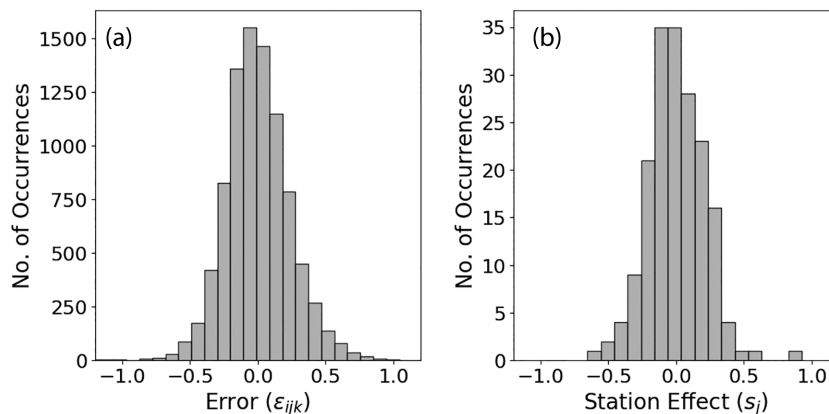


Figure 5. The distribution of (a) error terms (observed amplitudes – predicted amplitudes) and (b) station effects, s_j resulting from the ML^P determination calculation. The error axis in panel (a) has been truncated; a small number (~ 0.23 per cent) of observations have $|\epsilon_{ijk}| > 1.2$ s.

some geographically anomalous station effects cannot be explained by a low number of observations (leading to large uncertainties in the estimate), and appear to be station-specific effects. For example, the large negative station effect (-0.65) at station AEU

in East Anglia ($52.6202N, 1.2347E$) is constrained by 44 observations. Station corrections, ($S = -s_j$), for currently operational stations, and their 95 per cent confidence bounds, are provided in Table 3.

Table 3. Selected station corrections, S , used in the formulation of ML^P (eq. 9) and the associated 95 per cent confidence intervals. Only stations currently in the BGS broad-band network or the AWE Blacknest UKNET are listed.

Station	S	95 per cent C.I. (m.u.)	Station (m.u.)	S (m.u.)	95 per cent C.I. (m.u.)
BIGH	0.20	0.07,0.32	KPL	0.08	0.03,0.13
CCA1	0.04	-0.04,0.12	LAW	0.15	0.03,0.28
CLGH	0.20	0.09,0.31	LBWR	-0.15	-0.24,-0.06
CWF	0.10	0.06,0.14	LEWI	0.41	0.17,0.66
DRUM	0.03	-0.06,0.12	LMK	-0.27	-0.33,-0.21
DYA	0.07	0.01,0.13	LRW	0.15	-0.03,0.33
EDI	0.05	0.00,0.10	MCH1	0.03	0.00,0.07
EDMD	-0.07	-0.16,0.02	MONM	-0.11	-0.20,-0.03
ELSH	-0.25	-0.37,-0.14	NEWG	0.26	0.13,0.39
ESK	0.11	0.06,0.15	OLDB	-0.22	-0.31,-0.12
FOEL	0.07	0.00,0.14	PGB1	0.00	-0.05,0.05
GAL1	0.29	0.24,0.34	RSBS	0.50	0.38,0.63
GDLE	-0.15	-0.27,-0.03	STNL	-0.19	-0.27,-0.11
HLM1	0.16	0.12,0.20	STRD	-0.27	-0.35,-0.20
HMNX	-0.29	-0.43,-0.14	SWN1	-0.33	-0.38,-0.27
HPK	-0.17	-0.21,-0.13	WACR	-0.11	-0.21,-0.01
HTL	-0.03	-0.08,0.02	WLF1	0.06	0.00,0.11
INVG	0.35	0.23,0.46	LLW	0.45	0.32,0.58
IOMK	-0.10	-0.20,0.00	LPW	0.09	-0.02,0.20
JSA	-0.06	-0.14,0.02	SBD	0.07	0.02,0.11
KESW	0.09	0.02,0.16	WOL	-0.05	-0.15,0.05

4.2 Comparing ML^P and ML^{BGS}

A comparison of ML^{BGS} and ML^P estimates illustrates that at lower magnitudes ($ML^{BGS} \leq 3.1$) there is an approximately 1:1 correspondence between the two magnitude scales, but at higher magnitudes the ML^P values are reduced with respect to ML^{BGS} (Fig. 6a). In the absence of justification for a more complicated model, two orthogonal distance regressions are calculated to represent the relationships in regions of lower and higher ML^{BGS} :

$$ML^P = (0.94 \pm 0.16) ML^{BGS} + (0.15 \pm 0.40), \quad 2.0 \leq ML^{BGS} \leq 3.1, \quad (20)$$

$$ML^P = (0.73 \pm 0.13) ML^{BGS} + (0.78 \pm 0.51), \quad 3.1 < ML^{BGS} \leq 4.4, \quad (21)$$

where the quoted regression coefficient uncertainties are ± 1 standard deviation (± 1 s.d.). The uncertainties in ML^P are estimated as the standard distribution of the ML^P distribution at each ML^{BGS} value (Fig. 6a), while the uncertainties in ML^{BGS} were fixed at 0.1. The split between the two magnitude regions is chosen as $ML^{BGS} = 3.1$ because this is the magnitude above which the median ± 1 s.d. distributions of ML^P estimates do not always encompass the 1:1 correspondence line between the ML^{BGS} and ML^P scales (Fig. 6). Within uncertainties (both slope and intercept) the lower magnitude relationship cannot be distinguished from a 1:1 correspondence, while for the higher magnitude events the relationships are different (at the 1 s.d. level).

4.3 ML^P and ML^{BGS} for explosive events

ML^P and ML^{BGS} were calculated and compared for earthquake and explosion data sets (see Section 2). The median $ML^P - ML^{BGS}$ value equals 0.0 for the earthquake population; this is expected as the ML^P scale was generated using earthquake data and is tied to the ML^{BGS} scale by definition (eqs 13–16).

For events with an explosive component the median $ML^P - ML^{BGS}$ values are positive, although the variation around these median values is large (Fig. 7 and Table 4) such that the earthquake and explosion populations are not clearly separated. Explosions at sea exhibit a larger population separation, with $ML^P - ML^{BGS} = 0.50$ m.u. compared to a value of 0.21 m.u. for quarry explosions.

As there are only three on-land single-fired explosions within our database a distribution of $ML^P - ML^{BGS}$ values cannot be readily calculated, but it is observed that these events exhibit values of $ML^P - ML^{BGS} > 0.3$ (Fig. 8).

4.4 Across network scatter in magnitude estimates

Magnitude residuals (single station magnitude – averaged event magnitude) provide a measure of the magnitude scale consistency across the measurement network. For the earthquake and explosion populations studied in this paper (Section 2), magnitude residuals were calculated for both the ML^P and ML^{BGS} scales (Fig. 9). The ML^P estimates incorporate the calculated station corrections (Table 3), while the operational ML^{BGS} estimates do not include such terms. This difference explains the reduced standard deviation of the ML^P residual population (0.248 m.u.) when compared to ML^{BGS} (0.259 m.u.) for the earthquake population (Table 5). Ottemöller & Sargeant (2013) showed for a data set of 1482 observations that incorporating station terms into ML^{BGS} estimates reduced the magnitude residual standard deviation from 0.273 m.u. (comparable to the value found in our study) to 0.228 m.u.

For the explosion populations, the ML^P and ML^{BGS} magnitude residual standard deviations are similar (values within 0.01 m.u. of one another, Table 5), despite the ML^{BGS} estimates not incorporating station corrections. This is primarily due to a significant positive tail in the ML^P residual population for explosions (Fig. 9b) that increases the ML^P residual standard deviation. This positive tail corresponds to particular source to receiver paths that result

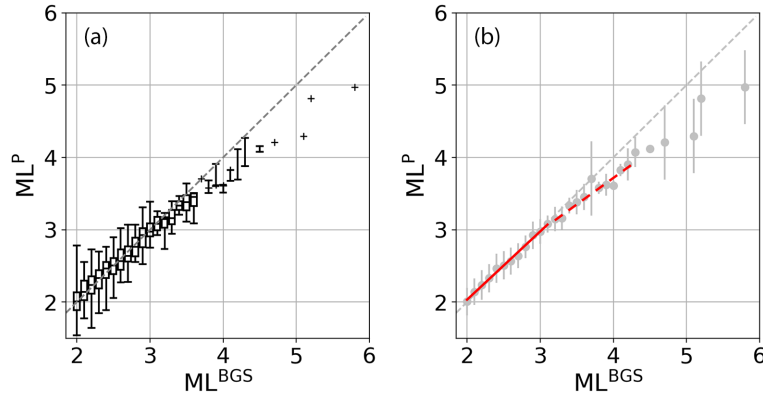


Figure 6. A comparison of the ML^{BGS} magnitudes with the ML^P magnitudes calculated in this study. Panel (a) provides a box and whisker plot of the calculated ML^P values in 0.1 m.u. wide bins of ML^{BGS} values. The lower and upper extent of the box are the 25th and 75th percentiles of the distribution, with the distribution limits shown by the whiskers; regions with only one data point are indicated by crosses. Panel (b) shows the same data, with median values as circles and $\pm 1\sigma$ given as bars (single point distributions are given arbitrary $1\sigma = 0.5$ m.u.) The regression lines detailed in eqs (20) and (21) are given by the solid and dashed red lines, respectively. The grey dashed line in both plots indicates the 1:1 correspondence line.

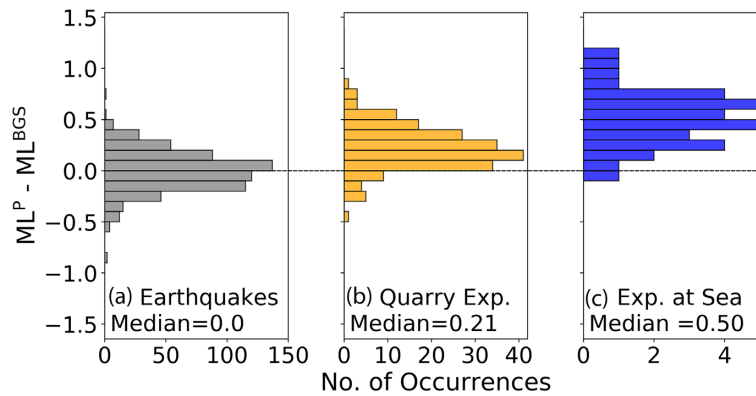


Figure 7. Histograms of the difference between ML^P and ML^{BGS} for all events within three categories: (a) the earthquakes from which the ML^P scale was constructed, (b) all quarry explosions (including those from the Glensanda quarry) and (c) all explosions at sea. The median difference between ML^P and ML^{BGS} values are provided on the plot; the value is zero for the earthquake population as this was one constraint placed on the generation of the ML^P scale.

Table 4. Median ($\widetilde{\Delta M}$) and standard deviation ($\sigma_{\Delta M}$) values for distributions of $\Delta M = ML^P - ML^{BGS}$ for different event populations (in magnitude units).

Data set	$\widetilde{\Delta M}$	$\sigma_{\Delta M}$
Earthquakes	0.00	0.19
Quarry explosions	0.21	0.21
Explosions at sea	0.50	0.27

in higher than average seismic amplitudes. For example, the set of significantly positive residuals between 310 and 360 km all correspond to paths between mining explosions near Buxton, Derbyshire and station SBD, Cornwall (at an azimuth of 214°). For the 15 explosive events for which *P* waves were recorded at SBD, five were in the Buxton area: these have a mean magnitude residual of 1.1 m.u. In contrast, the other 10 events, located across the southern UK and surrounding seas, exhibit a mean magnitude residual of 0.2 m.u.

5 DISCUSSION

The distance corrections determined for the ML^P scale provide insight into *P*-wave amplitude decay (consisting of both geometrical spreading and attenuation effects) across the UK (eqs 17 and 19).

Comparison of these results with *P*-wave studies in other tectonic regions is made difficult due to the low number of comparable studies, and the variety of frequency passbands used to calculate *P*-wave magnitudes. Acknowledging these difficulties, our results tentatively suggest that *P*-wave amplitude decay across the UK is low compared to other regions. The UK distance decay parameter of 1.8 (eq. 19) is smaller than values identified in tectonically stable regions such as France ($P_n:2.0, P_g:2.3$ for a passband centred on 5 Hz, Nicolas *et al.* 1982) and Brazil ($P:2.3$ for a 1–10 Hz passband, Assumpção 1983) and significantly smaller than that found in tectonically active Iran ($P_g:3.6$ at 1 Hz, Nuttli 1980).

Furthermore, Nuttli (1980) showed that for local and near-regional propagation across Iran the rate of amplitude decay of P_g and L_g phases could be considered to be identical. This is not the case for the UK (Fig. 4) where *P*-wave amplitude decay is significantly lower than for the L_g waves that dominate ML^{BGS} measurements. This is consistent with previous studies that have found higher shear wave (L_g) attenuation across Britain when compared to other stable tectonic areas (Sargeant & Ottemöller 2009; Ottemöller & Sargeant 2013).

The geographical differences in station terms (Fig. 3c) are consistent with the regional-scale geological variations across the UK: younger, weaker crustal sedimentary sequences in the south and east result in larger seismic amplitudes than the predominantly older, stronger igneous, metamorphic and sedimentary sequences in the

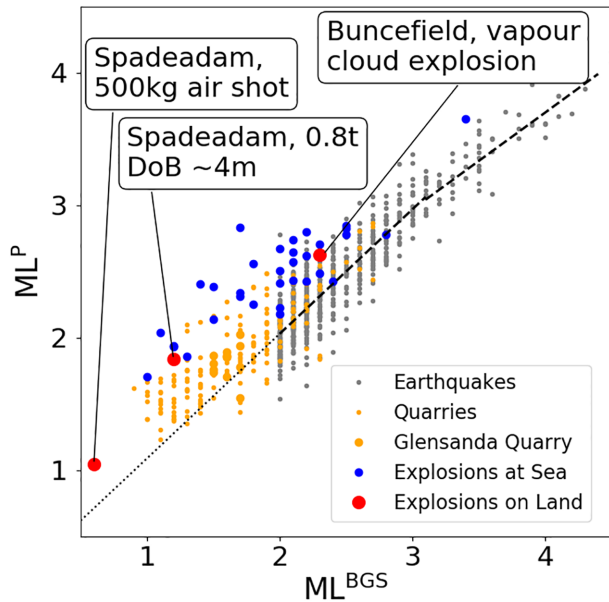


Figure 8. A comparison of ML^{BGS} and ML^P values for the explosion databases (coloured circles) and the earthquakes from which the ML^P relationship was calibrated (grey circles). The three explosions on land are annotated with their charge weight (TNT-equivalent) and emplacement condition (DoB = Depth of Burial). The Buncefield vapour cloud explosion does not have a known TNT-equivalent yield. The dashed line represents the $ML^{BGS}:ML^P$ relationship identified in Fig. 6. Only earthquakes with $ML^{BGS} \geq 2.0$ were used in the calculation of the ML^P scale (due to signal-to-noise ratio considerations); the dotted line represents an extrapolation of the $ML^{BGS}:ML^P$ relationship to lower magnitudes.

north and west which result in smaller seismic amplitudes. This is in general agreement with previous studies using S -wave amplitudes (Edwards *et al.* 2008; Ottemöller & Sargeant 2013). However, some differences exist; for example, our results exhibit signal deamplification in North-West Wales, while Edwards *et al.* (2008) show amplification. In addition, the stations on the Orkney Islands (North-East Scotland) exhibit small amounts of P -wave amplification while exhibiting S -wave deamplification (Edwards *et al.* 2008). Although a detailed investigation is outside the scope of this study, this indicates that differences in P - and S -wave attenuation may vary between localized regions of the UK, and that station-specific high-frequency amplification of P waves may be a significant effect at some sites. Moreover, we have assumed scenario-independent site effects. Recent work shows that site responses (and hence stations terms) depend significantly upon the frequency content of the impinging wavefield (Holt *et al.* 2019); scenario (earthquake size and epicentral distance) specific station terms may help reduce variance in magnitude estimates from across the sensor network.

For larger earthquakes ($ML^{BGS} > 3.1$), ML^{BGS} estimates are greater than the ML^P estimates (eqs 20 and 21, and Fig. 6). The potential for ML^P scale saturation was investigated as a potential cause, due to the more restricted ML^P measurement passband (generated using a four-pole high-pass Butterworth filter, with a corner frequency of 1.5 Hz) compared to the Wood–Anderson response used in the ML^{BGS} calculations (similar to a two-pole high-pass Butterworth filter, with a corner frequency of 2.0 Hz, Havskov & Ottemöller 2010). However, employing the methodology proposed by Deichmann (2006) to calculate ML saturation as a function of scalar moment, modified to use P -wave moment-rate functions (e.g.

Deichmann 1997), showed that ML^P and ML^{BGS} saturate in a similar manner. This is a result of the higher frequency content of the P -wave arrivals counteracting the sharper filter roll-off of the ML^P passband. Both scales begin to slowly saturate at $ML \sim 3$, with a simulated saturation effect of ~ 0.5 m.u. at $ML = 5$.

For larger earthquakes ($ML^{BGS} \gtrsim 3$), it is instructive to compare ML^{BGS} and ML^P estimates with moment magnitude (M_w) estimates that have been previously published for UK earthquakes (e.g. Sargeant & Ottemöller 2009; Ottemöller & Sargeant 2013). Fig. 10 compares the local magnitude estimates to M_w for 46 earthquakes, comprising the overlap between the data set used in this study and that of Sargeant & Ottemöller (2009) with the addition of the 2008 Market Rasen Earthquake M_w estimate (Ottemöller & Sargeant 2013). The ML^{BGS} to M_w relationship from this subset of events is consistent with those made in previous studies (Edwards *et al.* 2008; Sargeant & Ottemöller 2009; Ottemöller & Sargeant 2013). Orthogonal regressions, with equal errors of 0.1 m.u. given to all magnitude estimates, give,

$$M_w = (0.77 \pm 0.05) ML^{BGS} + (0.78 \pm 0.15), 2.7 \leq ML^{BGS} \leq 5.2, \quad (22)$$

$$M_w = (0.93 \pm 0.05) ML^P - (0.01 \pm 0.15), 2.4 \leq ML^P \leq 4.8 \quad (23)$$

where the quoted regression coefficient uncertainties are ± 1 standard deviation.

Previous studies (e.g., Edwards *et al.* 2008; Ottemöller & Sargeant 2013) have noted that the gradient of the ML^{BGS} to M_w relationship is consistently less than the value of one predicted by theory (Deichmann 2006), with the studies indicating that this is likely to be due to a combination of failing to correctly account for both source properties and S -wave attenuation across the UK. If the ML^{BGS} scale assumes too high an S -wave attenuation, the result is to predict significantly more along-path signal loss than actually occurred, such that the source magnitude must be overestimated to compensate (Edwards *et al.* 2008). In contrast, the gradient of the ML^P to M_w relationship is closer to one (eq. 23). If the attenuation terms for ML^P more accurately reflect the P -wave attenuation structure, this could account for the better correspondence with M_w when compared to ML^{BGS} . In addition, because the P -wave attenuation is significantly less than the S -wave attenuation (e.g. Fig. 4), ML^P estimates are likely to be less affected by biases caused by larger events having, on average, longer recording distances (and hence the larger magnitude events being affected more by differences between true and estimated attenuation parameters). This difference could help explain the divergence of the ML^P and ML^{BGS} scales at $ML^{BGS} > 3.1$. The ML^{BGS} estimates are increased compared to ML^P because distance-dependent overestimation of S -wave attenuation effects are increasing ML^{BGS} with respect to the earthquake source parameters (as parametrized by M_w), while ML^P continues to more accurately reflect these values. However, this remains conjecture; to further investigate these effects an accurate P -wave attenuation model for the UK would need to be constructed, and this is outside the scope of this study.

At lower magnitudes ($ML^{BGS} \lesssim 3.1$), the ML^{BGS} and ML^P estimates exhibit an almost 1:1 relationship (eq. 20 and Fig. 6). There is not a database of M_w estimates for UK events at these smaller sizes, but it has been shown that for smaller earthquakes ML estimates tend to be less than M_w (e.g. Dost *et al.* 2018) as a result of the high frequencies associated with these small events being rapidly attenuated. As explained by Deichmann (2017) this leads

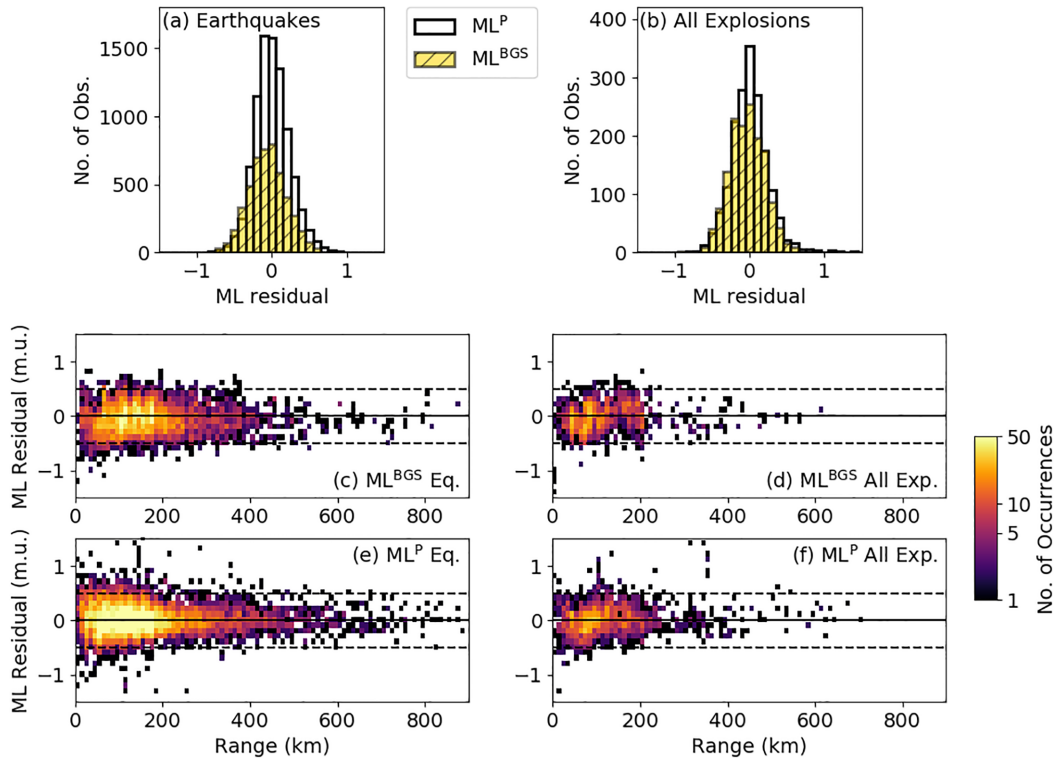


Figure 9. The distribution of magnitude residuals (station magnitude – event magnitude) for (a) the earthquake population and (b) the combined explosion population. Details of variances of the ML^{BGS} and ML^P residual populations are given in Table 5. Variations of the residual populations with range are given in panels (c) and (d) for the earthquakes (Eq.), and in panels (e) and (f) for all explosions (All Exp.). In these panels dashed horizontal lines are included at ± 0.5 m.u. for guidance only; they do not represent any physical limit.

Table 5. The standard deviations of the magnitude residual (station magnitude – event magnitude) populations (in magnitude units). The ML^P values always include a station correction, the operational ML^{BGS} values do not.

Data set	ML^{BGS}	ML^P
Earthquakes	0.259	0.248
All explosions	0.243	0.254
Quarry explosions	0.245	0.255
Explosions at sea	0.254	0.248

to the signals of small earthquakes being essentially the impulse response of the propagation medium scaled by the scalar moment. One hypothesis that may be useful to test in future studies is whether for small magnitude events both ML^{BGS} and ML^P scale with scalar moment, leading to the 1:1 correspondence between the scales for $ML^{BGS} \lesssim 3.1$.

A comparison of ML^P and ML^{BGS} values indicates that differences in *P*- and *S*-wave generation for earthquake and explosive source populations can be identified in $ML^P:ML^{BGS}$ ratios (e.g. Figs 7 and 8). However, due to the significant variance for individual event magnitudes, the power of network averaged magnitudes to discriminate between source types is low. This is to be expected; successful discrimination methods have required single station calibrations for magnitude and distance effects (Walter & Taylor 2001). A potential complication is that ML^{BGS} is not, by definition, an *S*-wave measure. In most cases it is, as L_g exhibits the largest amplitude arrival, but this is not always true (especially for explosive sources, e.g. Ottemöller and Evers 2008). In addition, the measurements that underpin ML^P and ML^{BGS} calculations contain significant energy below 3 Hz; optimal *P*:*S* discriminants often take advantage of differences in compressional and shear wavefield components

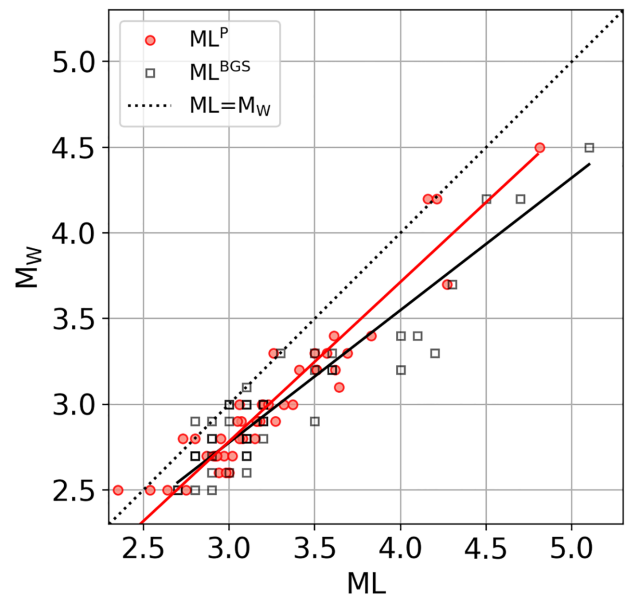


Figure 10. The relationship between the two local magnitude scales, ML^P and ML^{BGS} , and the M_w values calculated by Sargeant & Ottemöller (2009) and Ottemöller & Sargeant (2013) for 46 UK earthquakes with $ML^{BGS} > 2.7$. Solid red and black lines are resulting orthogonal regression fits to the ML^P and ML^{BGS} data (equal errors of 0.1 m.u. are assigned to all data points in both dimensions).

at higher frequencies (Walter *et al.* 2007). A quantitative understanding of how much discrimination power exists in $ML^P:ML^{BGS}$ ratios (or differences) would require further work to understand the

partitioning of errors inherent in the magnitude calculation process into model inadequacy and station noise terms, and whether any correlations exist between these errors (e.g. Anderson *et al.* 2009).

Results suggest that $ML^P - ML^{BGS}$ is reduced at higher magnitudes for underwater explosions (Fig. 7). Given the lack of knowledge of shot depth and water depth we are unable to assess whether this variation with magnitude is the result of variations in explosive emplacement conditions. However, studies of controlled underwater explosion series show little evidence for significant differences in shear wave energy generation with water depth (Willis 1963).

Interpreting the discrimination results is also complicated by the possible issue of data censoring. Due to the paucity of large events across the UK, the explosion data set has significant numbers of small events ($ML^P \leq 2$, Fig. 8). For the smaller events (i.e. lowest ML^{BGS}) P waves are more likely to be identified if they generate higher than average amplitudes, biasing the ML^P population to higher magnitudes. Quantitatively assessing such an effect is outside the scope of this study, but may be possible using a maximum-likelihood estimate for ML^P .

The ML^P magnitude scale developed in this study provides a measure of event size based upon the amplitude of a consistent seismic phase (P). This is in contrast with standard local magnitude calculations (e.g. ML^{BGS}) which may incorporate a mixture of phases. Combined with the observation that ML^P is sensitive to the enhanced generation of P waves from explosions, it might therefore be expected that ML^P would be better suited to providing a relative size estimate for explosive sources. However, the magnitude residuals (Section 4.4) do not support this; the ML^P estimates at individual stations do not show less variance than ML^{BGS} estimates. The major factor appears to be the higher sensitivity of P -wave amplitudes, compared to L_g amplitudes, to the specific source-to-receiver path. This suggests that the assumption of a 1-D distance correction is less applicable for the ML^P magnitude scale when compared to ML^{BGS} .

As with other local magnitude scales, there is no clear correspondence between ML^P and a measure of explosive source size. Despite this, a consistent magnitude scale may be related to source characteristics (e.g. an explosive charge weight) via an empirical relationship if well-characterized events are used as calibration points (e.g. Khalturin *et al.* 1998). Currently, there has been little success in doing so for the UK, primarily due to the small number of well understood explosive sources (e.g. Booth 2009).

One advantage of network averaged measures, of which the ML^P and ML^{BGS} scales are examples, is that they can be applied to small events that are only recorded on a subset of stations in the UK. A disadvantage is that the averaged 1-D distance corrections for ML^P (plus station corrections) do not explain a significant amount of the measured amplitude variability, as seen by the variance in the results and the amplitudes of the error term (Fig. 5). Improvements to source size estimation could be made by either constructing azimuthal- and distance-dependent station corrections (e.g. Walter & Taylor 2001), or by using a method that estimates the source moment (e.g. coda-derived moment magnitudes, Mayeda *et al.* 2003); for both methods the calibration of individual stations within the network would take significant effort.

6 CONCLUDING REMARKS

A local magnitude scale for the UK, ML^P , has been developed that allows event sizes to be consistently estimated based upon P -wave

amplitude measurements. This is particularly useful for small near-surface explosions for which P -wave arrivals dominate the seismic recordings. However, analysis of magnitude residuals for events with both ML^P and ML^{BGS} estimates suggest that the P -wave magnitude scale does not exhibit reduced variance compared to standard L_g -amplitude measures (ML^{BGS}). This is primarily due to larger variance in along-path P -wave amplitude decay. Despite this, ML^P can be considered a useful measure for characterizing small seismic events within the UK, especially as it provides some discrimination power between earthquakes and explosion sources. Furthermore, observations suggest that for larger earthquakes ($ML^{BGS} \gtrsim 3$), P -wave amplitude measurements across the UK (i.e. ML^P) may better reflect the source scalar moment (M_w) than S -wave amplitude measures (i.e. ML^{BGS}), although further investigation of UK P -wave attenuation structure is required to provide confidence in this hypothesis.

ACKNOWLEDGEMENTS

The authors thank the dedicated engineers who deploy, and maintain, the UK seismometer networks. DG thanks both Stuart and Alex Nippress for discussions throughout the project. The authors would also like to thank two reviewers, Lars Ottemöller and Ben Edwards, and the associate editor, Eiichi Fukuyama, for the care taken in producing insightful and helpful comments regarding the original submission.

REFERENCES

- Anderson, D.N., Walter, W.R., Fagan, D.K., Mercier, T.M. & Taylor, S.R., 2009. Regional multistation discriminants: magnitude, distance, and amplitude corrections, and sources of error, *Bull. seism. Soc. Am.*, **99**(2A), 794–808.
- Assumpção, M., 1983. A regional magnitude scale for Brazil, *Bull. seism. Soc. Am.*, **73**(1), 237–246.
- Bakun, W.H. & Joyner, W.B., 1984. The M_L scale in Central California, *Bull. seism. Soc. Am.*, **74**(5), 1827–1843.
- Bamford, D., Nunn, K., Prodehl, C. & Jacob, B., 1978. LISPB - IV. Crustal structure of northern Britain, *Geophys. J. Int.*, **54**(1), 43–60.
- Booth, D.C., 2007. An improved UK local magnitude scale from analysis of shear and L_g -wave amplitudes, *Geophys. J. Int.*, **169**, 593–601.
- Booth, D.C., 2009. The relationship between seismic local magnitude M_L and charge weight for UK Explosions, Technical report, British Geological Survey. OR/09/062.
- Butcher, A., Luckett, R., Verdon, J.P., Kendall, J.M., Baptie, B. & Wookey, J., 2017. Local magnitude discrepancies for near-event receivers: implications for the U.K. traffic-light scheme, *Bull. seism. Soc. Am.*, **107**(2), 532–541.
- Carpenter, E.W., Marshall, P.D. & Douglas, A., 1967. The amplitude distance curve for short period teleseismic P -waves, *Geophys. J. Int.*, **13**(1–3), 61–70.
- Deichmann, N., 1997. Far-field pulse shapes from circular sources with variable rupture velocities, *Bull. seism. Soc. Am.*, **87**(5), 1288–1296.
- Deichmann, N., 2006. Local magnitude, a moment revisited, *Bull. seism. Soc. Am.*, **96**(4A), 1267–1277.
- Deichmann, N., 2017. Theoretical basis for the observed break in M_L/M_w scaling between small and large earthquakes, *Bull. seism. Soc. Am.*, **107**(2), 505–520.
- Denny, M.D., Taylor, S.R. & Vergino, E.S., 1987. Investigation of m_b and M_S formulas for the Western United States and their impact on the M_S/m_b discriminant, *Bull. seism. Soc. Am.*, **77**(3), 987–995.
- Dost, B., Edwards, B. & Bommer, J.J., 2018. The relationship between M and ML : a review and application to induced seismicity in the Groningen Gas Field, The Netherlands, *Seismol. Res. Lett.*, **89**(3), 1062–1074.

- Douglas, A., 2001. The UK broadband seismology network, *Astron. Geophys.*, **42**(2), 2–19.
- Douglas, A., 2013. *Forensic Seismology and Nuclear Test Bans*, Cambridge University Press, Cambridge, UK.
- Edwards, B., Rietbrock, A., Bommer, J.J. & Baptie, B., 2008. The acquisition of source, path, and site effects from microearthquake recordings using Q tomography: application to the United Kingdom, *Bull. seism. Soc. Am.*, **98**(4), 1915–1935.
- Havskov, J. & Ottemoller, L., 2010. *Routine Data Processing in Earthquake Seismology: With Sample Data, Exercises and Software*, Springer Science & Business Media.
- Holt, J., Edwards, B. & Poggi, V., 2019. Scenario-dependent site effects for the determination of unbiased local magnitude, *Bull. seism. Soc. Am.*, **109**(6), 2658–2673.
- Khalturin, V.I., Rautian, T.G. & Richards, P.G., 1998. The seismic signal strength of chemical explosions, *Bull. seism. Soc. Am.*, **88**(6), 1511–1524.
- Lockett, R., Ottemöller, L., Butcher, A. & Baptie, B., 2019. Extending local magnitude M_L to short distances, *Geophys. J. Int.*, **216**(2), 1145–1156.
- Mayeda, K., Hofstetter, A., O’Boyle, J.L. & Walter, R.L., 2003. Stable and transportable regional magnitudes based on coda-derived moment-rate spectra, *Bull. seism. Soc. Am.*, **93**(1), 224–239.
- Nicolas, M., Massinon, B., Mechler, P. & Bouchon, M., 1982. Attenuation of regional phases in Western Europe, *Bull. seism. Soc. Am.*, **72**(6A), 2089–2106.
- Nuttli, O.W., 1980. The excitation and attenuation of seismic crustal phases in Iran, *Bull. seism. Soc. Am.*, **70**(2), 469–485.
- Ottemöller, L. & Evers, L.G., 2008. Seismo-acoustic analysis of the Buncefield Oil Depot Explosion in the UK, 2005 December 11, *Geophys. J. Int.*, **172**, 1123–1134.
- Ottemöller, L. & Sargeant, S., 2013. A local magnitude scale M_L for the United Kingdom, *Bull. seism. Soc. Am.*, **103**(5), 2884–2893.
- Richter, C.F., 1935. An instrumental earthquake magnitude scale, *Bull. seism. Soc. Am.*, **25**(1), 1–32.
- Sargeant, S. & Ottemöller, L., 2009. Lg wave attenuation in Britain, *Geophys. J. Int.*, **179**(3), 1593–1606.
- Vergino, E.S. & Mensing, R.W., 1990. Yield estimation using regional $m_b(p_n)$, *Bull. seism. Soc. Am.*, **80**(3), 656–674.
- Walter, W.R., Matzel, E., Pasyanos, M.E., Harris, D.B., Gok, R. & Ford, S.R., 2007. Empirical observations of earthquake-explosion discrimination using P/S ratios and implications for the sources of explosion S-waves, In *29th Monitoring Research Review: Ground-Based Nuclear Explosion Monitoring Technologies*, US: National Nuclear Security Administration and the Air Force Research Laboratory, pp. 685–693.
- Walter, W.R. & Taylor, S.R., 2001. A revised magnitude and distance amplitude correction (MDAC2) procedure for regional seismic discriminants: theory and testing at NTS, Technical Report UCRL-ID-146882, Lawrence Livermore National Lab., CA (USA).
- Willis, D.E., 1963. Seismic measurements of large underwater shots, *Bull. seism. Soc. Am.*, **53**(4), 789–809.